

# Multifunctional PtCuTe Nanosheets with Strong ROS Scavenging and ROS-Independent Antibacterial Properties Promote Diabetic Wound Healing

Yaru Guo, Shuai Ding, Changshuai Shang, Chenguang Zhang, Menggang Li, Qinghua Zhang, Lin Gu, Boon Chin Heng, Shihan Zhang, Feng Mei, Ying Huang, Xuehui Zhang, Mingming Xu, Jiuhui Jiang,\* Shaojun Guo,\* Xuliang Deng,\* and Lili Chen\*

Nanozymes, as one of the most efficient reactive oxygen species (ROS)-scavenging biomaterials, are receiving wide attention in promoting diabetic wound healing. Despite recent attempts at improving the catalytic efficiency of Pt-based nanozymes (e.g., PtCu, one of the best systems), they still display quite limited ROS scavenging capacity and ROS-dependent antibacterial effects on bacteria or immunocytes, which leads to uncontrolled and poor diabetic wound healing. Hence, a new class of multifunctional PtCuTe nanosheets with excellent catalytic, ROS-independent antibacterial, proangiogenic, anti-inflammatory, and immuno-modulatory properties for boosting the diabetic wound healing, is reported. The PtCuTe nanosheets show stronger ROS scavenging capacity and better antibacterial effects than PtCu. It is also revealed that the PtCuTe can enhance vascular tube formation, stimulate macrophage polarization toward the M2 phenotype and improve fibroblast mobility, outperforming conventional PtCu. Moreover, PtCuTe promotes crosstalk between different cell types to form a positive feedback loop. Consequently, PtCuTe stimulates a proregenerative environment with relevant cell populations to ensure normal tissue repair. Utilizing a diabetic mouse model, it is demonstrated that PtCuTe significantly facilitated the regeneration of highly vascularized skin, with the percentage of wound closure being over 90% on the 8th day, which is the best among the reported comparable multifunctional biomaterials.

most common complication of diabetes, has resulted in huge financial and social burdens on elderly patients. The etiology of chronic, nonhealing diabetic wounds is multifaceted, including uncontrolled accumulation of ROS, bacterial infection, microcirculatory perturbations, and sustained inflammation.<sup>[1,2]</sup> Among these, high ROS levels usually cause local irreversible oxidative damage, leading to the elevated inflammation and increased susceptibility to bacterial infection.<sup>[2]</sup> The scavenging of excessive ROS in diabetic wounds is a highly promising strategy to overcome stalled wound healing.<sup>[3,4]</sup> Various nanozymes have been developed to scavenge the ROS for reducing oxidative stress damage, due to their relatively easy preparation, high durability, and good physiochemical stability against harsh environments.<sup>[5,6,7]</sup> Despite recent attempts at improving the catalytic efficiency of Pt-based nanozymes (e.g., PtCu, one of the best systems), their ROS scavenging capacity is still unsatisfactory.<sup>[8]</sup> Moreover, ROS levels in different cell types are usually spatially heterogeneous. Specifically, ROS

## 1. Introduction

With rapidly aging populations and increasing prevalence of diabetes mellitus worldwide, impaired diabetic wound closure, the

at physiological levels is pivotal to the healthy functioning of endothelial cells (ECs) and fibroblasts, while phagocytic macrophages and neutrophils destroy the invading microbes through high ROS concentrations.<sup>[9,10]</sup> The regional

Y. Guo, S. Zhang, Y. Huang, X. Zhang, M. Xu, X. Deng  
Department of Geriatric Dentistry  
NMPA Key Laboratory for Dental Materials  
National Engineering Laboratory for Digital and Material  
Technology of Stomatology  
Beijing Laboratory of Biomedical Materials  
Peking University School and Hospital of Stomatology  
Beijing 100081, China  
E-mail: kqdengxuliang@bjmu.edu.cn

S. Ding, J. Jiang  
Department of Orthodontics  
Peking University School and Hospital of Stomatology  
National Clinical Research Center for Oral Diseases & National  
Engineering Laboratory for Digital and Material Technology of  
Stomatology  
Beijing Key Laboratory of Digital Stomatology  
Beijing 100081, China  
E-mail: kqjiangjiuhui@bjmu.edu.cn

 The ORCID identification number(s) for the author(s) of this article can be found under <https://doi.org/10.1002/adma.202306292>

DOI: 10.1002/adma.202306292

heterogeneity of ROS indicates that only scavenging ROS to the physiological level would inevitably damage the ROS-dependent antibacterial property.<sup>[11]</sup> Moreover, many nanozymes also exert their antibacterial effects through ROS generation in bacteria, which leads to the secondary damage of local tissues. Although many antioxidative biomaterials are often incorporated with antibiotics or other antibacterial molecules to enhance their antibacterial properties, their biosafety and effectiveness are quite limited.<sup>[12]</sup> Therefore, nanomaterials with both improved catalytic efficiency and ROS-independent antibacterial properties are highly desirable. However, searching for a new class of biomedical materials for achieving such a comprehensive effect, is still a formidable challenge.

Here, we report a new class of PtCuTe nanosheets with both strong ROS-scavenging capacity and good ROS-independent antibacterial properties for promoting diabetic wound healing. We find that our fabricated PtCuTe can not only promote angiogenesis, macrophage polarization toward a proregenerative M2 phenotype and fibroblast mobility, without incorporation of additives, but also enhance the crosstalk between ECs, macrophage and fibroblasts, thus forming a positive feedback loop to mitigate the pathological microenvironment (Figure 1). With a diabetic mice model and in vivo imaging system, the PtCuTe nanosheets can effectively promote diabetic wound healing, attaining a percentage of wound closure of up to 91% on day 8, which has not been achieved before by other comparable studies.

## 2. Results and Discussion

The synthesis of PtCuTe nanosheets was achieved by a solvothermal method using Pt(acac)<sub>2</sub>, Cu(CH<sub>3</sub>COO)<sub>2</sub>, and H<sub>6</sub>TeO<sub>6</sub> as metal precursors and citric acid as reductant, with the assistance of Mo(CO)<sub>6</sub>. The high-angle annular dark-field scanning transmission electron microscopy (HAADF-STEM) image (Figure 2a)

and high-resolution transmission electron microscopy (HRTEM) image (Figure S1, Supporting Information) of PtCuTe nanomaterials reveal that individual PtCuTe materials consists of several nanosheets with a lateral size of about 148 nm. HAADF-STEM images of the perpendicular and horizontal nanosheets (Figure 2b–d) clearly show the lamellar morphology, and regular alternating dark and bright spots. Due to the introduction of Cu with smaller radius, the lattice fringe spacings of (001) (0.511 nm) and (110) (0.196 nm) planes of PtCuTe are smaller than those of hexagonal-phase PtTe<sub>2</sub> (001) planes (0.522 nm) and (110) planes (0.201 nm).<sup>[13]</sup> These observations are in accordance with the result that the X-ray powder diffraction (XRD) peak of the (110) plane of PtCuTe is positively shifted (Figure 2f). Meanwhile, all the XRD peaks of PtCuTe are similar to those of PtTe<sub>2</sub> (18-0977), and no extra peak can be found (Figure 2f).<sup>[14]</sup> These pieces of evidence collectively confirm the successful embedding of Cu atoms into the PtTe<sub>2</sub> lattice. The elemental mapping discloses that Pt, Cu, and Te are distributed evenly throughout the nanomaterial (Figure 2g). The atomic ratio of Pt:Cu:Te is determined to be 28.5:10.8:60.7 by the inductively-coupled plasma-atomic emission spectroscopy (ICP-AES) (Figure 2h). X-ray photoelectron spectroscopy (XPS) of PtCuTe reveals that most Pt in the PtCuTe nanosheets exist in the oxidized states (Figure 2i; and Figure S2, Supporting Information) whereas that of PtCu nanoparticles exist in metallic states and their oxidized Cu atom amount is much lower (Figure S3, Supporting Information), revealing the strong electronic interactions between Te and other elements in PtCuTe nanosheets.

The ROS scavenging capacities of PtCuTe and PtCu nanomaterials were investigated, including •OH scavenging capacity, peroxidase (POD)-like, catalase (CAT)-like, and superoxide dismutase (SOD)-like activity. First, the •OH scavenging capacities of PtCuTe and PtCu were tested with electron paramagnetic resonance (EPR) technique. The peak intensities of •OH gradually decreased with increasing PtCuTe and PtCu dosages, while relatively weaker intensities in the PtCuTe group were found at all their selected same concentrations (Figure 2j,k), revealing the stronger catalytic scavenging activity of PtCuTe to •OH. The POD-like activity was evaluated by the use of 3, 3', 5, 5'-tetramethylbenzidine (TMB) as the chromogenic substrate. As shown in Figure 2l, the absorbance at 652 nm of the system with PtCuTe is much higher than that of the PtCu system, indicating that PtCuTe nanosheets have the superior POD-like activity. Moreover, PtCuTe exhibits efficient CAT-like and SOD-like activities (Figure S4, Supporting Information). The above results thus indicate that the PtCuTe nanosheets show stronger ROS scavenging activity.

Diabetic wounds are more prone to bacterial infection, and ROS plays a key role in host defense. Phagocytic macrophages and neutrophils destroy invading microbes in their phagosomes though the release of high-concentration ROS. Due to the excellent ROS scavenging capacity of PtCuTe nanosheets, we next investigated whether PtCuTe exerted its antibacterial function in a ROS-independent manner. For this purpose, SOD and CAT were used throughout bacterial culture to maintain the ROS at a low level. The coating dilution plate experiment and counting of colony-forming units (CFUs) showed that the staphylococcus aureus (*S. aureus*) colony units significantly decreased after the PtCuTe treatment for 24 h in a concentration-dependent

C. Shang, M. Li, S. Guo  
School of Materials Science and Engineering  
Peking University  
Beijing 100871, China  
E-mail: guosj@pku.edu.cn

C. Zhang  
Hospital of Stomatology  
Guanghua School of Stomatology  
Sun Yat-Sen University  
Guangzhou 528406, China

Q. Zhang, L. Gu  
Beijing National Laboratory for Condensed Matter Physics  
Institute of Physics  
Chinese Academy of Sciences  
Beijing 100190, China

B. C. Heng  
Central Laboratory  
Peking University School and Hospital of Stomatology  
Beijing 100081, China

F. Mei, L. Chen  
Department of Stomatology  
Union Hospital  
Tongji Medical College  
Huazhong University of Science and Technology  
Wuhan 430022, China  
E-mail: chenlili1030@hust.edu.cn

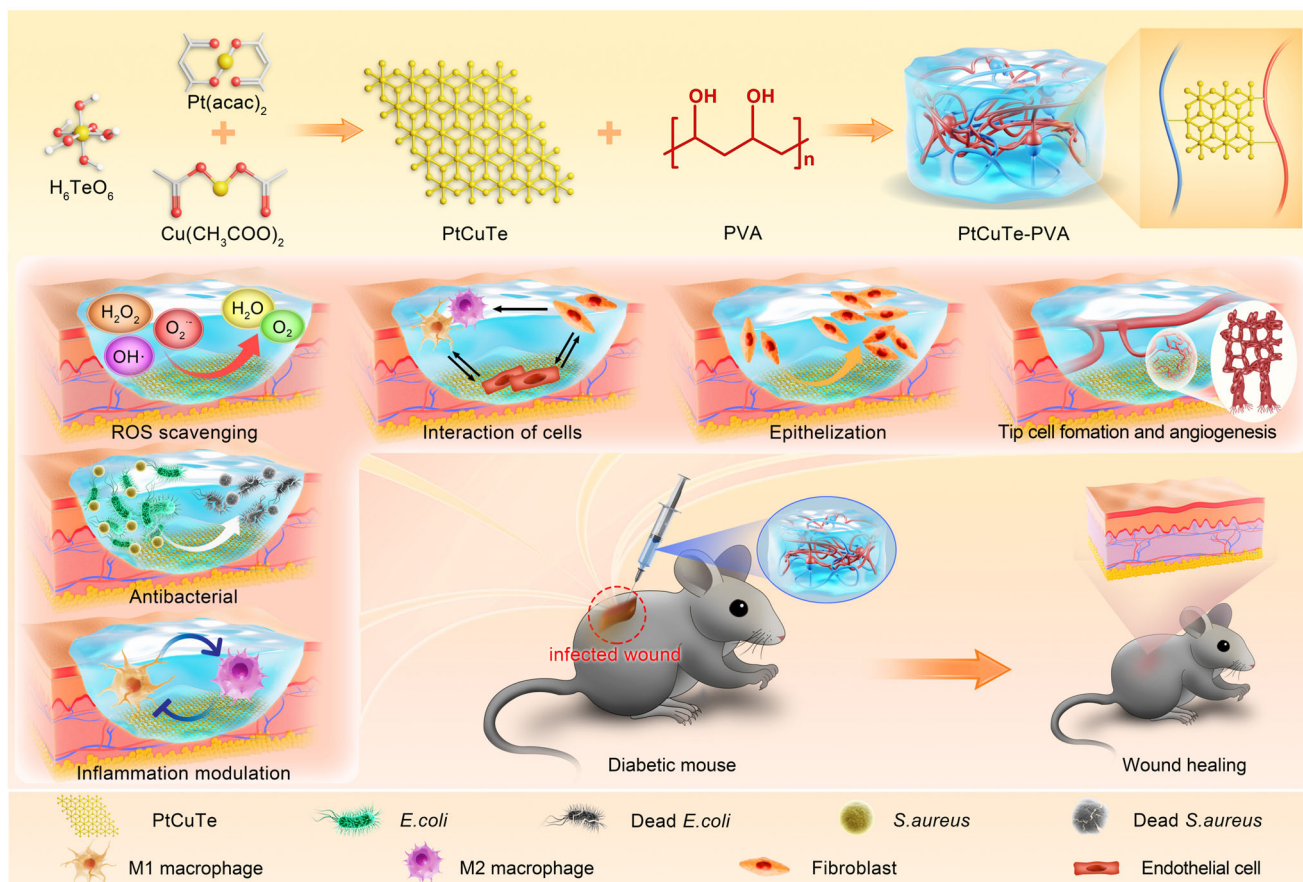


**Figure 1.** Schematic illustration of using PtCuTe nanosheets for treatment of diabetic wounds.

manner ( $0.25\text{--}2\ \mu\text{g mL}^{-1}$ , **Figure 3a,b**). As a comparison, more bacterial colony units were observed in the PtCu group. The results revealed the superior antibacterial activity of PtCuTe compared to the well-known PtCu nanoenzyme. Consistently, with live/dead staining assay of *S. aureus* (**Figure 3c**), we also found that the PtCuTe group had a significantly lower percentage of live bacteria (green fluorescence), whereas the bacteria in the PtCu group were mostly viable, thus demonstrating the better antibacterial ability of PtCuTe compared to that of PtCu. Additionally, the SEM and TEM results showed that almost all *S. aureus* treated with PtCuTe lost their normal cell membrane structures and began to rupture, while PtCu treatment had a negligible impact on the integrity of bacterial cell membranes (**Figure 3d**). Taken together, these results thus indicated the excellent ROS-independent antibacterial performance of PtCuTe. The superior antimicrobial properties of PtCuTe to PtCu were further confirmed by the anti-*Escherichia coli* (*E. coli*) assay (**Figure S5**, Supporting Information), showing the strong *E. coli* killing ability of PtCuTe by disrupting bacterial membrane integrity. Our results are consistent with previous studies that the antibacterial activity of Te and telluride relies mainly on membrane damage and flagellar movement inhibition, rather than ROS production and DNA damage.<sup>[15,16]</sup> Compared to other current antibacterial agents, which eliminate bacteria via external physical stimuli (e.g., light, sound, microwaves),

PtCuTe nanosheets exhibits more flexibility in antibacterial applications.

The biocompatibility of PtCuTe and its intracellular antioxidant activity at selected concentrations were then investigated. Live/dead staining, ethynyl-deoxyuridine, and cell counting kit-8 assays (**Figures S6–S8**, Supporting Information) demonstrated the superior biocompatibility of PtCuTe, exhibiting very minimal detrimental effects on the survival and proliferation of human umbilical vein endothelial cells (hUVECs), THP-1, and fibroblasts. CellROX deep red reagent was used as the fluorescent probe to investigate the ROS-scavenging capacity of PtCuTe against intracellular ROS. After incubating hUVECs with D-glucose (25 mM), a strong red fluorescence signal can be observed, indicating a high level of intracellular ROS under high glucose (HG) conditions. By contrast, red fluorescence signals were dramatically attenuated in a concentration-dependent manner when hUVECs+D-glucose were treated with different concentrations of PtCuTe and PtCu. The quantitative analysis revealed that the ROS signals in the PtCuTe group were lower than those in the PtCu group at all selected concentrations (**Figure S9**, Supporting Information). Similar tendencies were also found by flow cytometry (**Figure S10**, Supporting Information), showing that PtCuTe treatment significantly decreased the percentage of ROS-positive hUVECs. Taken together, PtCuTe exhibits intracellular antioxidant capacity more strongly than PtCu, thus

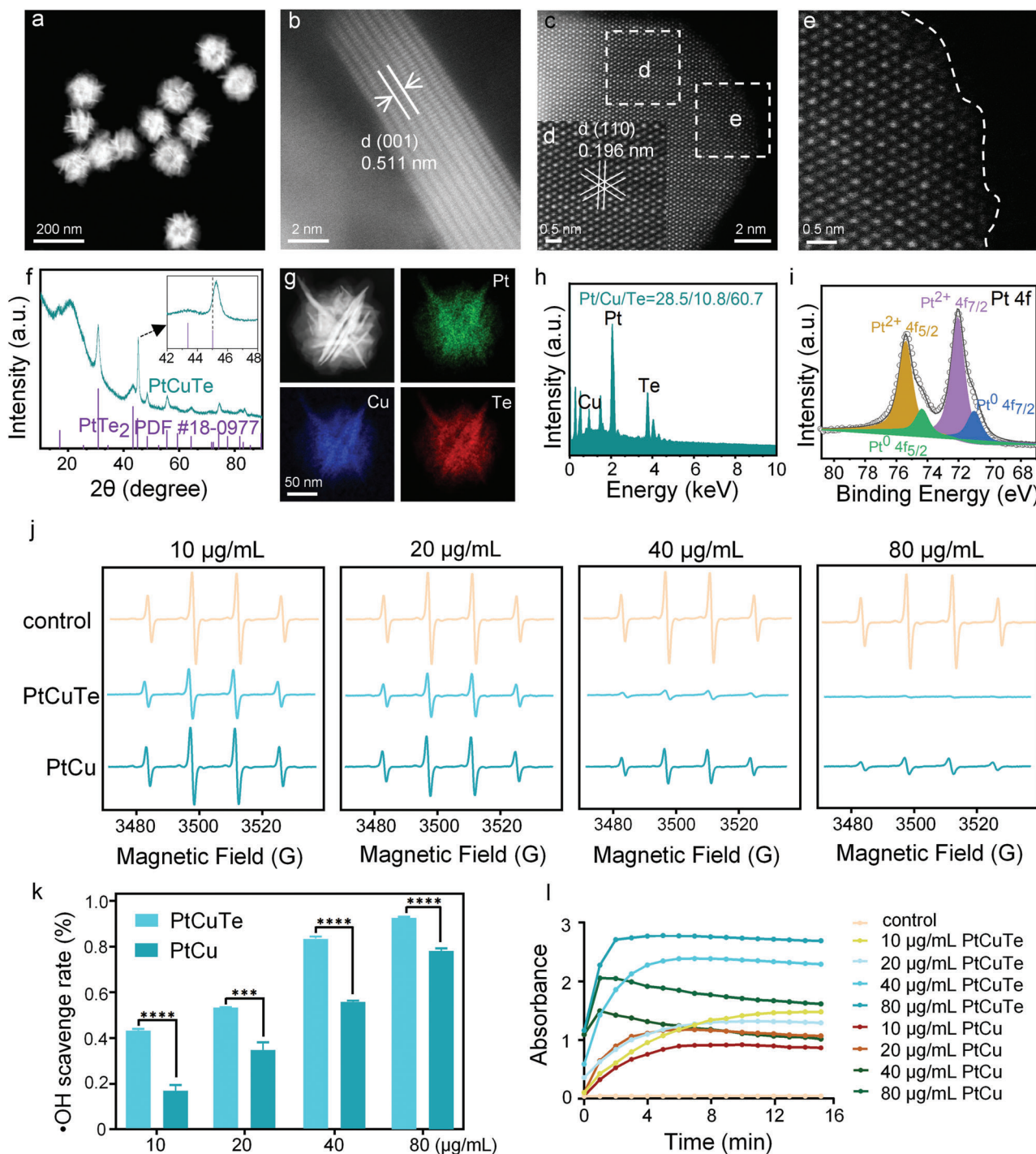


**Figure 2.** Characterization of PtCuTe nanosheets and their ROS scavenging capacity in vitro. a–e) Typical HAADF-STEM images (a–e), XRD pattern (f), EDS mapping (g), SEM-EDS (h), and Pt 4f XPS spectrum (i) of PtCuTe nanosheets. j) EPR spectroscopy and k) quantitative analysis of  $\bullet\text{OH}$  after PtCuTe and PtCu treatment. l) The time-dependent absorbance curves of the oxidation of TMB by  $\text{H}_2\text{O}_2$  catalyzed by different concentrations of PtCuTe and PtCu. (Dashed lines in (e) were used to mark the irregular edges of PtCuTe nanosheets).

indicating its significant potential for reducing oxidative damage in diabetic wounds.

Diabetes-induced endothelial dysfunction is a critical and initiating factor in the pathogenesis of diabetic vascular complications. After confirming excellent biocompatibility of PtCuTe and

its efficient ROS scavenging capacity, we then investigated the effect of PtCuTe on endothelial functions. Through the tube formation assay, we found that the vessel tube formation of hU-VECs was significantly hindered in the HG group (Figure 4a), which was accompanied by a decrease in the total tubule length,

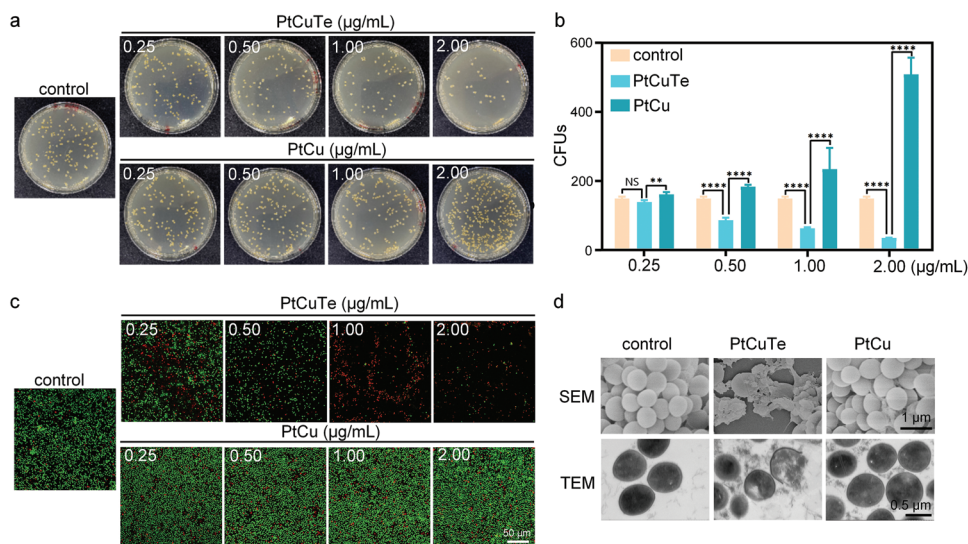


**Figure 3.** PtCuTe displayed strong antibacterial activity. a) Representative images of *S. aureus* colonies with different treatment. b) Quantitative analysis of *S. aureus* colonies in (a). c) Live/dead staining of *S. aureus* in different treatment groups. d) Representative SEM and TEM images of *S. aureus* treated by 1 μg mL<sup>-1</sup> PtCuTe and PtCu.

number of junctions and tubules (Figure 4b). This impaired angiogenic phenotype was restored by PtCu and PtCuTe nanomaterials in a concentration-dependent manner, showing the best proangiogenic effect at a dose of 0.5 μg mL<sup>-1</sup> (Figure 4a,b). However, the hUVECs treated with PtCuTe displayed a significantly stronger tube formation ability at all tested concentrations. At 0.5 μg mL<sup>-1</sup>, PtCuTe exhibited a 1.8-fold, 1.4-fold, and 1.3-fold increase in lumen number, junction number, and lumen length, as compared to the PtCu group, respectively. Hence, it can be seen that PtCuTe promoted the angiogenic capacity of hUVECs to the level of normal glucose (NG) group, while PtCu only partly mitigated the impaired angiogenesis within the HG environment.

To gain deeper insights, we investigated the underlying mechanism of the proangiogenic effects of PtCuTe. Revascularization of the skin defect area requires functional specification of ECs into leading tip cells.<sup>[17]</sup> Immunofluorescence staining and flow cytometry analysis of the cell membrane protein CD34, the canonical marker of tip cells,<sup>[18]</sup> showed that HG condition significantly decreased CD34 expression and CD34<sup>+</sup> phenotype, while this decline was mitigated upon treatment with PtCuTe, with optimal effects at a concentration of 0.25 and 0.5 μg mL<sup>-1</sup> (Figure 4c,d; and Figures S11 and S12, Supporting Information). In addition, reverse transcription polymerase chain reaction (qRT-PCR) showed that the tip-cell-enriched gene transcripts after PtCuTe treatment (1 μg mL<sup>-1</sup>), including *Aplin*, *VEGFR2*, *IGF2*, *EFNB2*, and *DLL4*, displayed 48.6-folds, 23.5-folds, 14.6-folds, 7.9-folds, and 6.4-folds increases, respectively, compared with the HG group (Figure 4d; and Figure S13, Supporting Information). These results thus demonstrate that PtCuTe promotes the tip cell phenotype and specification, further confirmed by the increased sprout number and invasion distance of PtCuTe in the spheroid-based angiogenesis assay (Figure 4e,f; and Figure S14, Supporting Information).

Besides tip cell specification, EC migration is also essential for angiogenesis, and collective cell migration is a hallmark of wound repair.<sup>[19]</sup> We found that the collective EC migration was

hindered under the HG environment. On the contrary, PtCuTe treatment markedly enhanced the migration of collective ECs, as manifested by increased migration areas and radius lengths, as well as enhanced number of cells migrating from the 3D EC spheroids (Figure S15, Supporting Information). Our results indicate that PtCuTe promotes angiogenesis through enhancement of tip cell formation and increased mobility of ECs. Although excessive ROS causes oxidative stress, ROS at physiological level is pivotal in the normal wound-healing response, including angiogenic sprouts, antimicrobial activity, and immunomodulation.<sup>[11]</sup> The intracellular ROS levels with 2 μg mL<sup>-1</sup> of PtCuTe treatment were significantly lower than those in the control group (Figures S9 and S10, Supporting Information). This excessive ROS clearance might account for the decline in angiogenic performance at elevated PtCuTe concentration.

Besides endothelial dysfunction, another important feature of diabetic wound is the impaired transition of macrophages from “pro-inflammatory” (M1) to “pro-healing” (M2) phenotypes, resulting in a persistent proinflammatory environment.<sup>[20–22]</sup> As a result, the persistent nonresolving inflammation in a HG environment, characterized by increased M1 phenotype macrophages and elevated levels of proinflammatory cytokines (Figure 5a,b), contributes to impaired diabetic wound healing. Upon treatment with PtCuTe (0.5 μg mL<sup>-1</sup>), the proportion of M2 (CD206<sup>+</sup>) macrophages is increased, while the proportion of M1 (CD86<sup>+</sup>) macrophages is decreased (Figure 5a), accompanied with reduced secretion of IL-1β, IL-6, and TNF-α to the levels in the control group (Figure 5b). By contrast, PtCu exerted minimal effects on the polarization and proinflammatory cytokines expression of macrophages under the HG environment (Figure 5a,b).

With normalization of angiogenesis and immune microenvironment in a HG environment, normal wound healing also calls for the migration of fibroblasts.<sup>[23]</sup> Normally, fibroblasts must migrate to the wound bed before they can exert their functions effectively, including breaking down the fibrin clot,

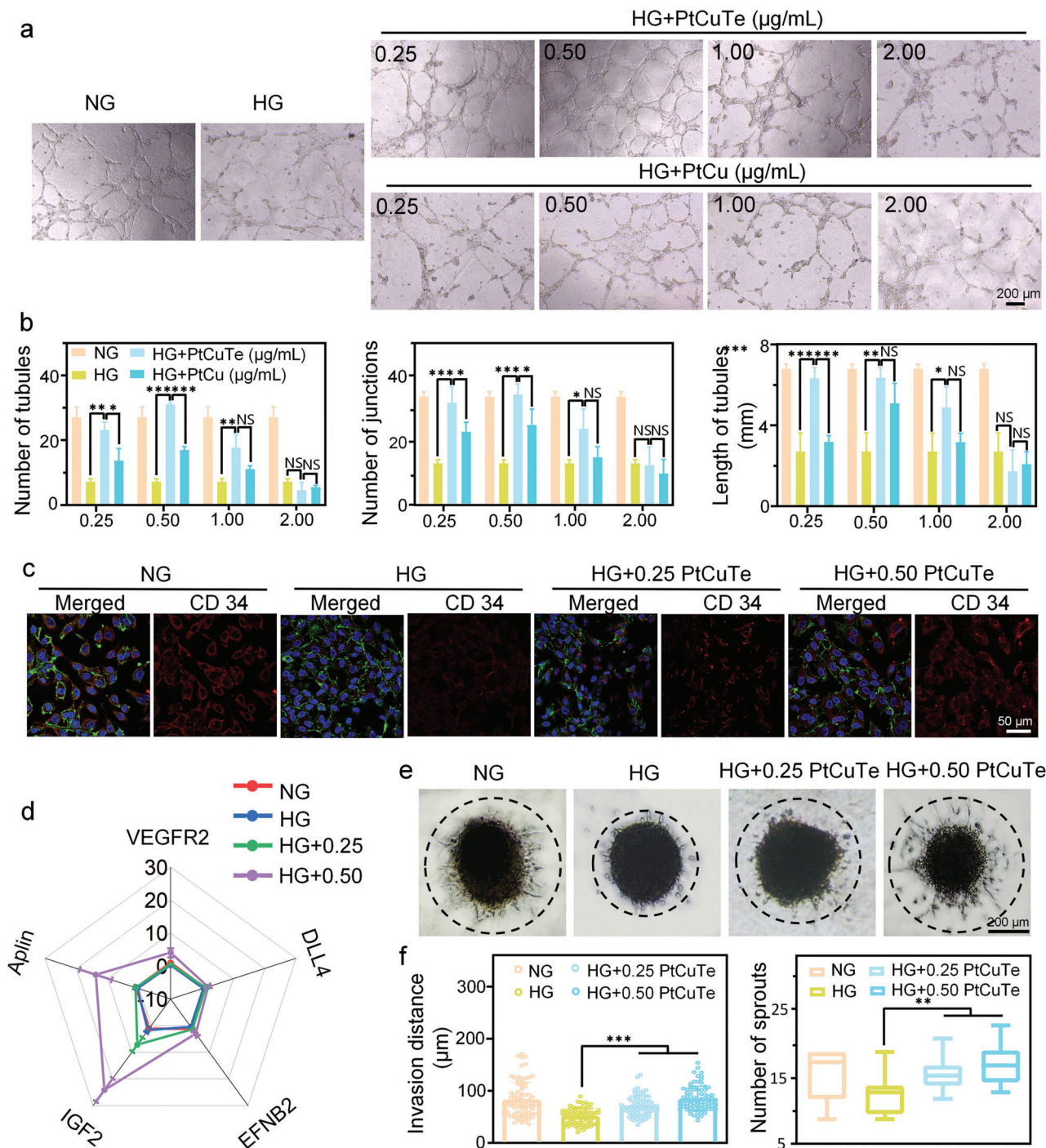


**Figure 4.** PtCuTe promoted angiogenesis and tip cell formation in vitro. a) Tube formation assay of hUVECs involving treatment with different concentrations PtCuTe and PtCu. b) Number of tubules, number of junctions, and total tube length in each group in (a). c) Immuno-fluorescence staining of tip cell marker CD34 in the different groups. d) qRT-PCR results of tip cell-enriched gene expression in the different treatment groups. e) Sprouting angiogenesis of hUVEC spheroids in the different treatment groups. f) Invasion distance and sprout number in each group in (e).

laying down new extracellular matrix, and providing the contractile forces to bring the wound edges together.<sup>[24]</sup> To quantify the cell migration speed, single cell tracking of fibroblasts was performed. Figure 5c shows the representative field of cell migration trajectories and centered trajectories of fi-

broblasts in every group with the cellular instantaneous velocity in different colors (blue representing lower speed and green to red representing higher speed). The short migration trajectories ( $64.39 \pm 23.80 \mu\text{m}$ ) and clustered blue speed ( $0.085 \pm 0.043 \mu\text{m min}^{-1}$ ) in the HG group indicate impaired

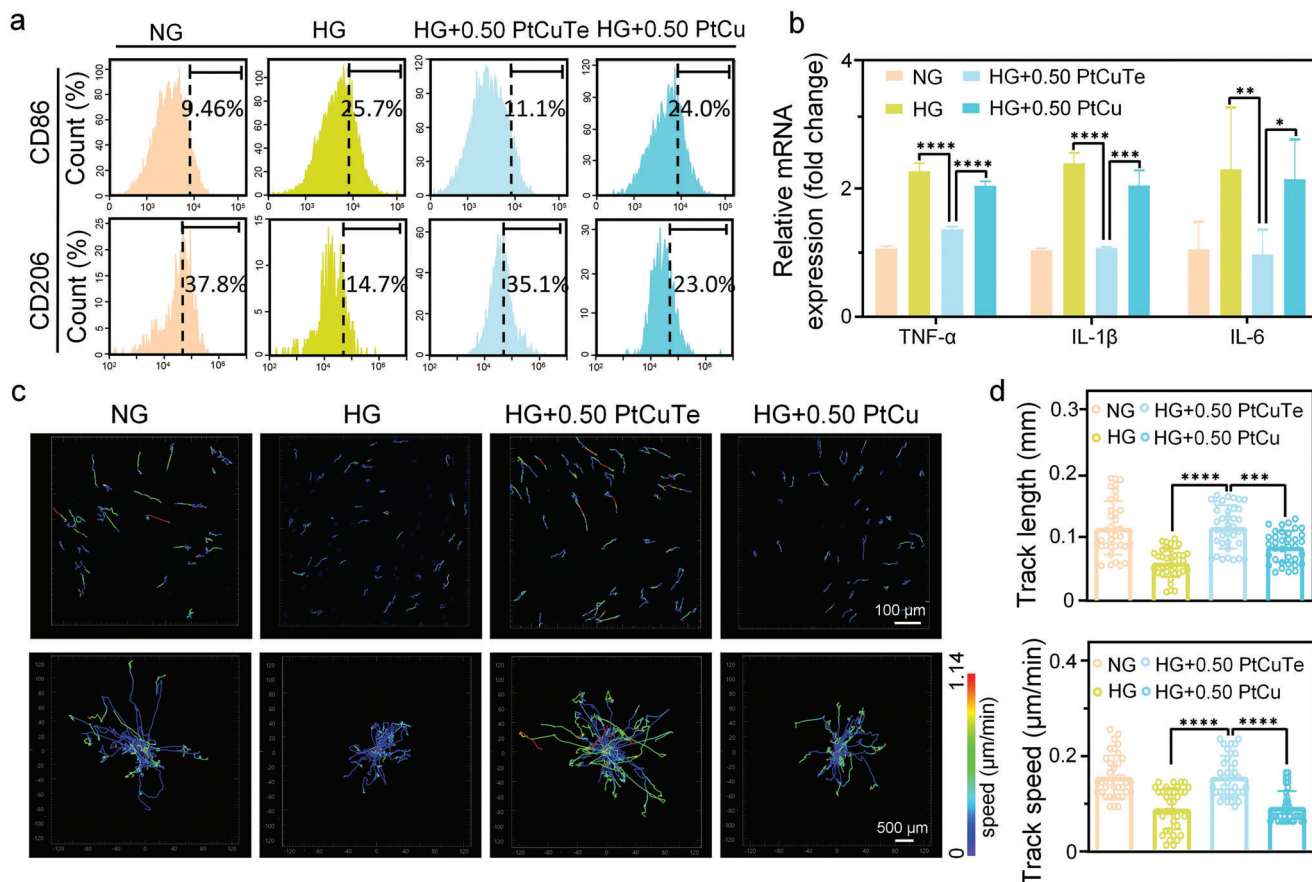


**Figure 5.** PtCuTe inhibited inflammation and enhanced fibroblast mobility. a) Flow cytometry results of CD86 and CD206, indicating that PtCuTe upregulated M2 and downregulated M1 macrophage polarization. b) PtCuTe inhibited the expression of proinflammatory factors, including TNF- $\alpha$ , IL-1 $\beta$ , and IL-6. c) Representative fields of cell migration trajectories and centered trajectories of fibroblasts in the different treatment groups. d) Quantification of fibroblast mobility, showing that the track length and track speed of fibroblasts were improved by PtCuTe treatment to the level of the control group.

fibroblast mobility (Figure 5c,d). After PtCuTe treatment, long migratory trajectories ( $124.95 \pm 36.29 \mu\text{m}$ ) and clustered green to red speed ( $0.152 \pm 0.042 \mu\text{m min}^{-1}$ ) were found, similar to those of the control group ( $123.43 \pm 44.92 \mu\text{m}$  and  $0.151 \pm 0.044 \mu\text{m min}^{-1}$  for migration length and instantaneous speed, respectively). In contrast, PtCu exerted negligible effects on migration trajectories ( $91.63 \pm 26.31 \mu\text{m}$ ) and instantaneous velocity ( $0.089 \pm 0.032 \mu\text{m min}^{-1}$ ) of HG-treated fibroblasts. The same phenomenon was also found in the scarification assay (Figure S16, Supporting Information), showing that PtCuTe-treated fibroblasts ( $0.5 \mu\text{g mL}^{-1}$ ) migrated closer toward the middle of the wound, as compared to the PtCu group and improved the wound closure rate to the level of the control group. These results thus indicate that fibroblast mobility impaired by the HG environment was completely restored by PtCuTe instead of PtCu.

Having confirmed the functional improvements of hUVECs, macrophages and fibroblasts by PtCuTe, we next explored the crosstalk among these three types of wound healing-involved cells. Tube formation assay with conditioned medium (CM) of macrophages and fibroblasts in the different groups showed that PtCuTe treatment increased the angiogenic capacity of HG-treated ECs to the level of the control group, including the number of tubules and junctions as well as the length of tubules

(Figures S17a,b and S18a,b, Supporting Information), all of which were better than those of macrophages treated with PtCu. Previous studies have shown that prohealing macrophages can stimulate angiogenesis, and thus bridge initial inflammation and later tissue regeneration and repair.<sup>[25]</sup> Similarly, as the most abundant and critical cell type in the wound healing process,<sup>[26]</sup> fibroblasts are also capable of upregulating angiogenic factors, such as hepatocyte growth factor and vascular endothelial growth factor (VEGF).<sup>[27]</sup> The enzyme-linked immunosorbent assay of CM shows that PtCuTe treatment mitigated the decrease in VEGF secretion of HG-treated macrophages and fibroblasts, while PtCu exerted limited effects on mitigating decreased VEGF expression (Figures S14c and S15c, Supporting Information). Conversely, newly-formed blood vessels transport more macrophages and fibroblasts to the damaged area. Therefore, PtCuTe enhanced the crosstalk between ECs, macrophages, and fibroblasts, thus forming a positive feedback to promote diabetic wound healing.

Finally, we investigated whether PtCuTe could enhance infected diabetic wound healing in vivo. Infected wounds were created on diabetic mouse dorsal skin (Figure 6a). Representative images of the infected wounds in different groups (Figure 6b) demonstrated that diabetes delayed wound healing, and new

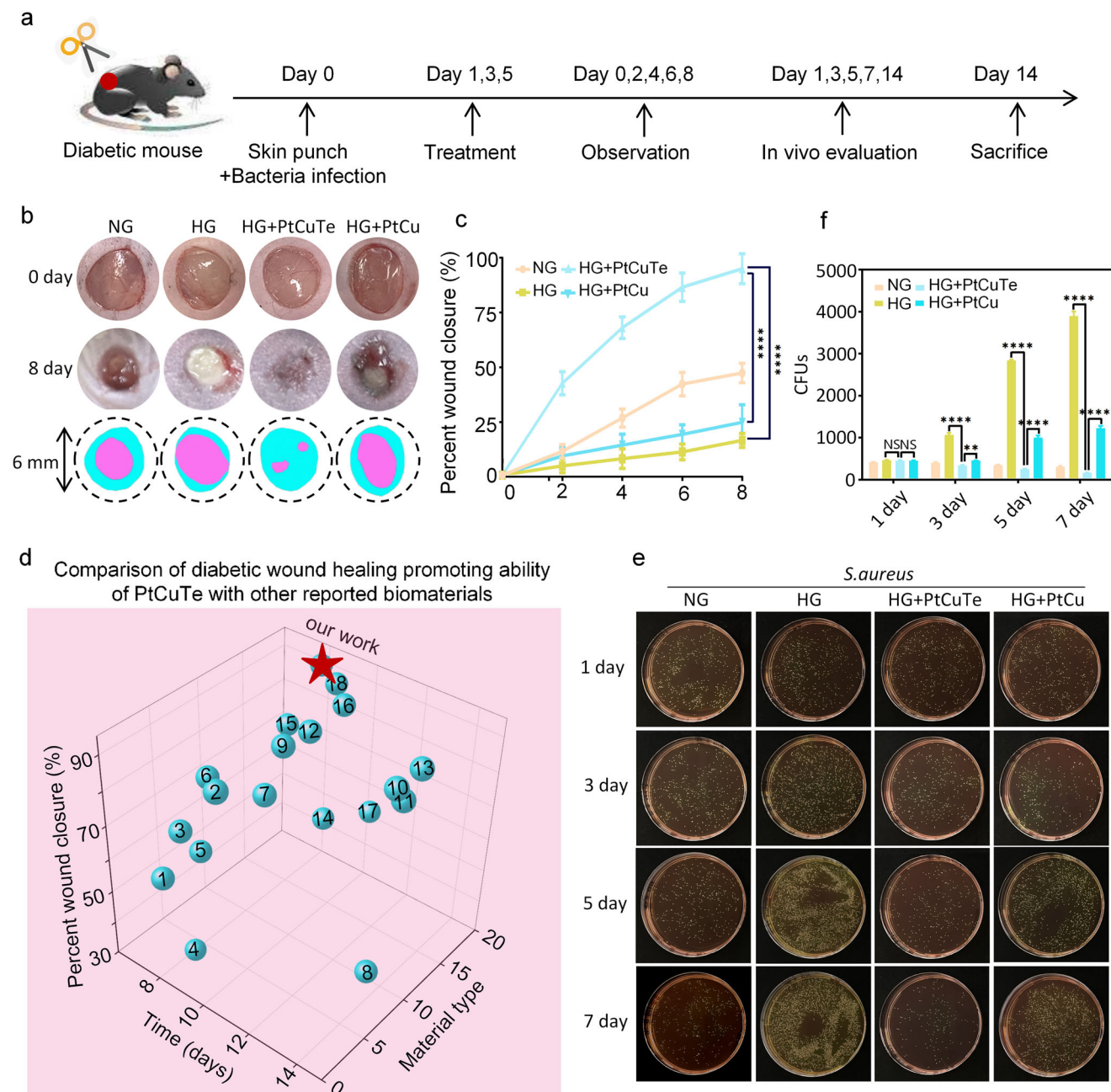


**Figure 6.** PtCuTe enhanced infected diabetic wound healing in vivo. a) Establishment of mouse skin defect model and the following treatment schedule. b) Representative images of the wound on day 0 and day 8 postwounding. The wound healing boundary on day 0 and day 8 postwounding is overlaid on the image. c) Quantification of the process of wound healing in all groups. d) Comparison of diabetic wound healing promoting capacity of PtCuTe with other published materials.<sup>[2,3,28–43]</sup> e) Representative images of *S. aureus* colonies in the different groups. f) Quantitative analysis of *S. aureus* colonies in (e).

tissue formation was significantly increased by the PtCuTe nanosheets. As shown in Figure 6b,c, the wound healing in diabetic mice only achieved about 10% closure on day 6 and 15% closure on day 8, significantly lower than that of the healthy mice (40% and 45% on day 6 and 8, respectively). After treatment with PtCuTe nanosheets, the wound closure percentage increased to 83% on day 6, 91% on day 8. However, 23% closure of skin wound on day 8 in PtCu group indicated that the traditional PtCu showed

limited effects on infected diabetic wound healing. Similarly, the wound closure percentage values of PtCuTe are also much higher than those recently reported metals or metal-oxide-based ROS-scavenging biocatalysts and other organic materials (Figure 6d), including studies with and without bacterial infection.<sup>[2,3,28–43]</sup>

In order to evaluate the antibacterial effect of PtCuTe in vivo, sterile swabs were used to collect *S. aureus* and *E. coli* around the wounds on day 1, 3, 5, and 7, and the bacterial burden was

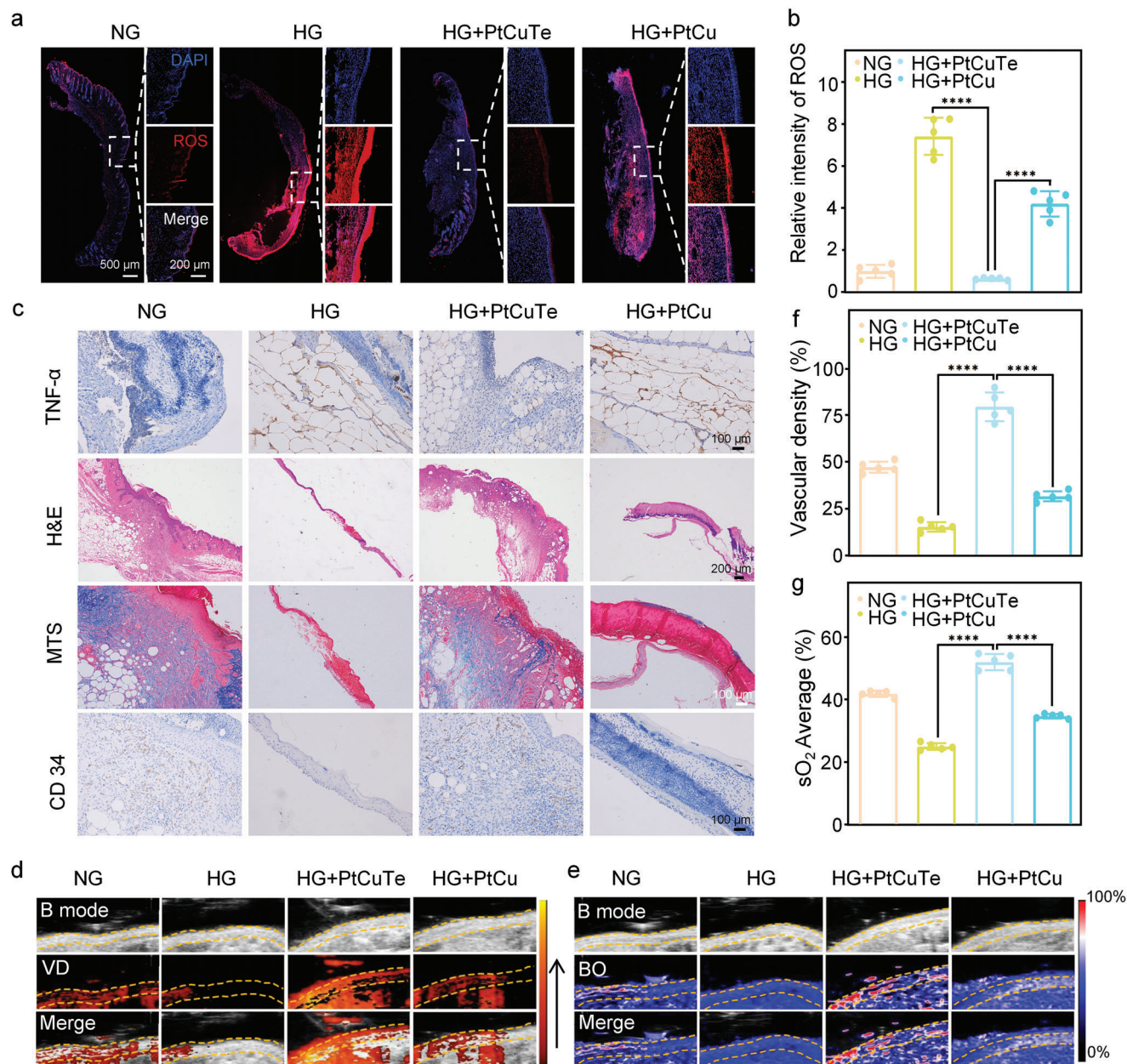


**Figure 7.** Wound microenvironment changes induced by PtCuTe treatment. a) ROS immunofluorescence staining of skin wound tissue in different groups. b) Quantitative analysis of ROS in (a). c) H&E staining (on day 7), MTS (on day 7), and IHC (TNF- $\alpha$  on day 3 and CD34 on day 7) of wound tissues. Ultrasound and PA images of VD in (d) and BO in (e) in different groups. f) Quantitative analysis of VD in (d). g) Quantitative analysis of BO in (e).

determined by enumerating the bacterial counts on Mannitol Agar and MacConkey Salt Agar plates (Figure 6e; and Figure S19, Supporting Information). As expected, the number of bacterial colonies in the PtCuTe group (145 CFUs for *S. aureus* and 26 CFUs for *E. coli* on day 7) was slightly lower than NG group (300 CFUs for *S. aureus* and 53 CFUs for *E. coli* on day 7), and much lower than that in the HG (4118 CFUs for *S. aureus* and 683 CFUs for *E. coli* on day 7) and PtCu (1276 CFUs for *S. aureus* and 525 CFUs for *E. coli* on day 7) groups. Consistent with the in vitro results, the animal studies demonstrated

that PtCuTe treatment exhibited excellent antibacterial activity in vivo.

Then skin slice analysis was performed to evaluate antioxidative, anti-inflammatory, wound healing promotion (including re-epithelialization and collagen deposition) and proangiogenic abilities of PtCuTe nanosheets. The intracellular ROS levels in vivo were monitored by fluorescence staining (Figure 7a,b). A dramatically diminished red fluorescence was observed as a result of dressing PtCuTe nanosheets compared with HG and PtCu groups, indicating its stronger ROS clearance

ability than PtCu. Immunohistochemical staining of IL-1 $\beta$ , IL-6, and TNF- $\alpha$  on day 3 after surgery showed that the expression levels of these inflammatory factors in the control and PtCuTe group were significantly lower than those in the diabetic and PtCu groups (Figure 7c; and Figure S20, Supporting Information), thus revealing the anti-inflammatory effects of PtCuTe during the process of diabetic mice wound healing. Immunohistochemistry was also performed to explore the effects of PtCuTe on macrophage phenotype modulation, showing that PtCuTe increased the macrophages with the M2 phenotype (CD68<sup>+</sup>CD206<sup>+</sup>) and decreased the M1 phenotype macrophages (CD68<sup>+</sup>CD86<sup>+</sup>) compared with the diabetic and PtCu groups (Figure S21, Supporting Information). In addition, hematoxylin and eosin (H&E) staining (Figure 7c; and Figure S22, Supporting Information) and Masson's trichrome staining (MTS, Figure 7c; and Figure S23, Supporting Information) indicated that faster re-epithelialization and better collagen deposition were achieved with PtCuTe treatment, superior to the negative group.

Microvascularization is the only means to transport nutrients and remove metabolic wastes in tissues, and thus is an important indicator of the wound healing process.<sup>[44]</sup> Therefore, the staining of CD34 (a marker of newly-formed vessels), vascular density (VD), and the blood oxygenation level (an indicator of functional blood vessel formation) were evaluated through immunohistochemistry (IHC) and photoacoustic (PA) imaging system to examine proangiogenic performance of PtCuTe nanosheets. Intense positive CD34 staining was observed in the PtCuTe group, and significantly higher than that in the HG and PtCu groups (Figure 7c). Cross-sectional PA and ultrasound images on day 14 (Figure 7d,e) showed the blood flow and oxygen saturation (sO<sub>2</sub>) around the wound site. Consistent with the IHC results, wounds treated with PtCuTe showed improved recovery with abundant blood perfusion and a markedly higher average blood oxygen (BO) level. As illustrated in the quantitative analysis in Figure 7f,g, diabetic environment decreased the VD average from 45.83% in control group to 14.61% and sO<sub>2</sub> average from 41.66% to 24.81%. After treated with PtCuTe, VD average and sO<sub>2</sub> average were improved to 77.35% and 51.74%, respectively, significantly higher than those in the PtCu group (30.58% for VD average and 34.49% for sO<sub>2</sub> average). These results collectively reveal that the PtCuTe nanosheets could effectively accelerate wound healing, eliminate bacteria, reduce inflammation, and promote angiogenesis, which are remarkably superior to traditional PtCu nanoenzyme. All animal surgical procedures were approved by the Institutional Animal Care and Use Committee of Peking University (No. LA2022660).

### 3. Conclusion

We have developed a new class of PtCuTe nanosheets for the promotion of diabetic wound healing. We found that PtCuTe showed stronger ROS scavenging capacity and better ROS-independent antibacterial properties than conventional PtCu-based materials. It promoted endothelial tip cell formation, enhanced vascular tube formation, stimulated macrophage polarization toward the M2 phenotype and improved fibroblast mobility. Moreover, PtCuTe enhanced the crosstalk between different cells, forming a positive feedback loop to stimulate a proregenerative environment enriched with proangiogenic factors, with relevant cell pop-

ulations to facilitate normal tissue repair. Consequently, by using a full-thickness skin defect model in diabetic mice, we found that PtCuTe application achieved significant accelerated wound healing at a rate not reported before.

### Supporting Information

Supporting Information is available from the Wiley Online Library or from the author.

### Acknowledgements

Y.G., S.D., and C.S. contributed equally to this work. This work was supported by the National Natural Science Foundation of China (Nos. 81991505, U22A20160, 82221003, 82201123 and 22105007), the National Key R&D Program of China (No. 2021YFC2400404), Beijing Natural Science Foundation (No. 30307472319), Peking University School of Stomatology National Clinical Key Discipline Construction Project (No. PKUSSNKP-T202101), and China Postdoctoral Science Foundation (Nos. 2021M700279, 2023T160029 and 2020M670018).

### Conflict of Interest

The authors declare no conflict of interest.

### Data Availability Statement

The data that support the findings of this study are available from the corresponding author upon reasonable request.

### Keywords

angiogenesis, diabetes mellitus, nanosheets, reactive oxygen species, wound healing

Received: June 29, 2023

Revised: August 22, 2023

Published online:

- [1] V. Falanga, *Lancet* **2005**, *366*, 1736.
- [2] H. Zhao, J. Huang, Y. Li, X. Lv, H. Zhou, H. Wang, Y. Xu, C. Wang, J. Wang, Z. Liu, *Biomaterials* **2020**, *258*, 120286.
- [3] J. Chen, Y. Liu, G. Cheng, J. Guo, S. Du, J. Qiu, C. Wang, C. Li, X. Yang, T. Chen, Z. Chen, *Small* **2022**, *18*, 2201300.
- [4] S. Huang, S. Xu, Y. Hu, X. Zhao, L. Chang, Z. Chen, X. Mei, *Acta Biomater.* **2022**, *137*, 199.
- [5] X. Mou, Q. Wu, Z. Zhang, Y. Liu, J. Zhang, C. Zhang, X. Chen, K. Fan, H. Liu, *Small Methods* **2022**, *6*, 2200997.
- [6] X. Ren, D. Chen, Y. Wang, H. Li, Y. Zhang, H. Chen, X. Li, M. Huo, *J. Nanobiotechnol.* **2022**, *20*, 92.
- [7] Q. Tian, W. Wang, L. Cao, X. Tian, G. Tian, M. Chen, L. Ma, X. Liu, Z. Yuan, C. Cheng, Q. Guo, *Adv. Mater.* **2022**, *34*, 2207275.
- [8] Y. Liu, Y. Qing, L. Jing, W. Zou, R. Guo, *Langmuir* **2021**, *37*, 7364.
- [9] C. Dahlgren, H. Bjornsdottir, M. Sundqvist, K. Christenson, J. Bylund, *Methods Mol. Biol.* **2020**, *2087*, 301.
- [10] F. C. Fang, *Nat. Rev. Microbiol.* **2004**, *2*, 820.
- [11] M. P. Brynildsen, J. A. Winkler, C. S. Spina, I. C. MacDonald, J. J. Collins, *Nat. Biotechnol.* **2013**, *31*, 160.

- [12] C. Tu, H. Lu, T. Zhou, W. Zhang, L. Deng, W. Cao, Z. Yang, Z. Wang, X. Wu, J. Ding, F. Xu, C. Gao, *Biomaterials* **2022**, *286*, 121597.
- [13] H. Ma, P. Chen, B. Li, J. Li, R. Ai, Z. Zhang, G. Sun, K. Yao, Z. Lin, B. Zhao, R. Wu, X. Tang, X. Duan, X. Duan, *Nano Lett.* **2018**, *18*, 3523.
- [14] C. Shang, Q. Wang, H. Tan, S. Lu, S. Wang, Q. Zhang, L. Gu, J. Li, E. Wang, S. Guo, *JACS Au* **2022**, *2*, 2453.
- [15] A. Tang, Q. Ren, Y. Wu, C. Wu, Y. Cheng, *Int. J. Mol. Sci.* **2022**, *23*, 11697.
- [16] A. Mohanty, M. H. Kathawala, J. Zhang, W. N. Chen, J. S. C. Loo, S. Kjelleberg, L. Yang, B. Cao, *Biotechnol. Bioeng.* **2014**, *111*, 858.
- [17] J. Kim, Y. H. Kim, J. Kim, D. Y. Park, H. Bae, D. Lee, K. H. Kim, S. P. Hong, S. P. Jang, Y. Kubota, Y. Kwon, D. Lim, G. Y. Koh, *J. Clin. Invest.* **2017**, *127*, 3441.
- [18] M. J. Siemerink, I. Klaassen, I. M. Vogels, A. W. Griffioen, C. J. Van Noorden, R. O. Schlingemann, *Angiogenesis* **2012**, *15*, 151.
- [19] P. Friedl, D. Gilmour, *Nat. Rev. Mol. Cell Biol.* **2009**, *10*, 445.
- [20] R. E. Mirza, M. M. Fang, W. J. Ennis, T. J. Koh, *Diabetes* **2013**, *62*, 2579.
- [21] R. E. Mirza, M. M. Fang, E. M. Weinheimer-Haus, W. J. Ennis, T. J. Koh, *Diabetes* **2014**, *63*, 1103.
- [22] Y. Xiong, Z. Lin, P. Bu, T. Yu, Y. Endo, W. Zhou, Y. Sun, F. Cao, G. Dai, Y. Hu, L. Lu, L. Chen, P. Cheng, K. Zha, M. A. Shahbazi, Q. Feng, B. Mi, G. Liu, *Adv. Mater.* **2023**, *22*, 2212300.
- [23] Y. Guan, H. Niu, Z. Liu, Y. Dang, J. Shen, M. Zayed, L. Ma, J. Guan, *Sci. Adv.* **2021**, *7*, eabj0153.
- [24] T. Wong, J. A. McGrath, H. Navsaria, *Br. J. Dermatol.* **2007**, *156*, 1149.
- [25] G. C. Rowe, S. Raghuram, C. Jang, J. A. Nagy, I. S. Patten, A. Goyal, M. C. Chan, L. X. Liu, A. Jiang, K. C. Spokes, D. Beeler, H. Dvorak, W. C. Aird, Z. Arany, *Circ. Res.* **2014**, *115*, 504.
- [26] S. Mahmoudi, E. Mancini, L. Xu, A. Moore, F. Jahanbani, K. Hebestreit, R. Srinivasan, X. Li, K. Devarajan, L. Prélôt, C. E. Ang, Y. Shibuya, B. A. Benayoun, A. L. S. Chang, M. Wernig, J. Wysocka, M. T. Longaker, M. P. Snyder, A. Brunet, *Nature* **2019**, *574*, 553.
- [27] S. W. Kim, G. B. Im, G. J. Jeong, S. Baik, J. Hyun, Y. J. Kim, C. Pang, Y. C. Jang, S. H. Bhang, *Biomaterials* **2021**, *275*, 120954.
- [28] J. Chen, D. Chen, J. Chen, T. Shen, T. Jin, B. Zeng, L. Li, C. Yang, Z. Mu, H. Deng, X. Cai, *Acta Biomater.* **2022**, *146*, 49.
- [29] Y. Guan, H. Niu, Z. Liu, Y. Dang, J. Shen, M. Zayed, L. Ma, J. Guan, *Sci. Adv.* **2021**, *7*, eabj0153.
- [30] T. Wang, Y. Li, E. J. Cornel, C. Li, J. Du, *ACS Nano* **2021**, *15*, 9027.
- [31] P. L. Thi, Y. Lee, D. L. Tran, T. T. H. Thi, J. I. Kang, K. M. Park, K. D. Park, *Acta Biomater.* **2020**, *103*, 142.
- [32] J. Mei, J. Zhou, L. Kong, Y. Dai, X. Zhang, W. Song, C. Zhu, *J. Nanobiotechnol.* **2022**, *20*, 232.
- [33] M. Yin, J. Wu, M. Deng, P. Wang, G. Ji, M. Wang, C. Zhou, N. T. Blum, W. Zhang, H. Shi, N. Jia, X. Wang, P. Huang, *ACS Nano* **2021**, *15*, 17842.
- [34] Y. Xiong, L. Chen, P. Liu, T. Yu, C. Lin, C. Yan, Y. Hu, W. Zhou, Y. Sun, A. C. Panayi, F. Cao, H. Xue, L. Hu, Z. Lin, X. Xie, X. Xiao, Q. Feng, B. Mi, G. Liu, *Small* **2022**, *18*, 2104229.
- [35] J. Liu, M. Qu, C. Wang, Y. Xue, H. Huang, Q. Chen, W. Sun, X. Zhou, G. Xu, X. Jiang, *Small* **2022**, *18*, 2106172.
- [36] S. Kuang, F. He, G. Liu, X. Sun, J. Dai, A. Chi, Y. Tang, Z. Li, Y. Gao, C. Deng, Z. Lin, H. Xiao, M. Zhang, *Biomaterials* **2021**, *275*, 120963.
- [37] C. Wei, P. Tang, Y. Tang, L. Liu, X. Lu, K. Yang, Q. Wang, W. Feng, Q. T. H. Shubhra, Z. Wang, H. Zhang, *Adv. Healthcare Mater.* **2022**, *11*, 2200717.
- [38] Y. He, K. Liu, S. Guo, R. Chang, C. Zhang, F. Guan, M. Yao, *Acta Biomater.* **2023**, *155*, 199.
- [39] N. Kim, H. Lee, G. Han, M. Kang, S. Park, D. E. Kim, M. Lee, M. J. Kim, Y. Na, S. Oh, S. J. Bang, T. S. Jang, H. E. Kim, J. Park, S. R. Shin, H. D. Jung, *Adv. Sci.* **2023**, *10*, 2300816.
- [40] G. Li, C. Ko, D. Li, C. Yang, W. Wang, G. Yang, C. Di Primo, V. K. W. Wong, Y. Xiang, L. Lin, D. Ma, C. Leung, *Nat. Commun.* **2021**, *12*, 3363.
- [41] J. Ishihara, A. Ishihara, K. Fukunaga, K. Sasaki, M. J. V. White, P. S. Briquez, J. A. Hubbell, *Nat. Commun.* **2018**, *9*, 2163.
- [42] W. Srifa, N. Kosaric, A. Amorin, O. Jadi, Y. Park, S. Mantri, J. Camarena, G. C. Gurtner, M. Porteus, *Nat. Commun.* **2020**, *11*, 2470.
- [43] X. Wu, D. Huang, Y. Xu, G. Chen, Y. Zhao, *Adv. Mater.* **2023**, *35*, 2301064.
- [44] X. Zhang, J. Gan, L. Fan, Z. Luo, Y. Zhao, *Adv. Mater.* **2023**, *14*, 2210903.